

Inclusive K^+ -meson production in proton-nucleus interactions

M. Büscher^{1a}, V. Koptev², M. Nekipelov^{1,2}, Z. Rudy³, H. Ströher¹, Yu. Valdau^{1,2}, S. Barsov², M. Hartmann¹, V. Hejny¹, V. Kleber¹, N. Lang⁴, I. Lehmann¹, S. Mikirtychiants², and H. Ohm¹

¹ Institut für Kernphysik, Forschungszentrum Jülich, 52425 Jülich, Germany

² High Energy Physics Department, Petersburg Nuclear Physics Institute, 188350 Gatchina, Russia

³ Institute of Physics, Jagellonian University, Reymonta 4, 30059 Cracow, Poland

⁴ Institut für Kernphysik, Universität Münster, W.-Klemm-Str. 9, 48149 Münster, Germany

Received: date / Revised version: date

Abstract. The production of K^+ -mesons in pA ($A = D, C, Cu, Ag, Au$) collisions has been investigated at the COOLER SYnchrotron COSY-Jülich for beam energies $T_p = 1.0 - 2.3$ GeV. Double differential inclusive pC cross sections at forward angles $\vartheta_{K^+} < 12^\circ$ as well as the target-mass dependence of the K^+ -momentum spectra have been measured with the ANKE spectrometer. Far below the free NN threshold at $T_{NN} = 1.58$ GeV the spectra reveal a high degree of collectivity in the target nucleus. From the target-mass dependence of the cross sections at higher energies, the repulsive in-medium potential of K^+ -mesons can be deduced. Using pN cross-section parameterisations from literature and our measured pD data we derive a cross-section ratio of $\sigma(pn \rightarrow K^+ X)/\sigma(pp \rightarrow K^+ X) \sim (3 - 4)$.

PACS. 13.75.-n Hadron-induced low- and intermediate-energy reactions and scattering – 25.40.-h Nucleon-induced reactions and scattering

1 Overview

One important topic of contemporary hadron physics is the investigation of the influence of the nuclear medium on the properties of hadrons and their production processes. Such phenomena can, for example, be studied in detail by measuring meson production in proton-nucleus (pA) collisions. If the measurements are carried out at projectile energies below the threshold for free nucleon-nucleon (NN) collisions (so-called subthreshold production) these processes necessarily imply collective effects involving several of the nucleons inside the target nucleus. K^+ -production is particularly well suited for such investigations since this meson is heavy compared to the pion, so that its production requires strong medium effects. As a consequence, the production of K^+ -mesons in proton-nucleus collisions is an appropriate tool to learn either about cooperative nuclear phenomena or high momentum components in the nuclear many-body wave function.

In this paper we present data obtained at the ANKE spectrometer [1] of COSY-Jülich on inclusive K^+ production with various targets and over a wide range of beam energies, see Sects. 3 and 5. A simple parameterisation, in terms of a few Lorentz-invariant variables, is presented in Sect. 4 which allows us to compare our data, measured at near-forward angles $\vartheta < 12^\circ$, with those obtained in other experiments under different kinematical conditions. It is

shown that the data, in particular our results obtained at the lowest beam energy $T_p = 1.0$ GeV [2], reveal a large collective behavior of the target nucleons. Either large intrinsic momenta of the nucleons must be involved in the K^+ -formation processes or the number of participating nucleons must be significantly larger than one. The latter could, for example, be due to multi-step processes.

Final state interactions (FSI) of the produced particles in the residual nucleus can mask the information about the production mechanisms. For K^+ -mesons FSI effects are generally considered to be rather small, due to the strangeness being $S = +1$. As a consequence the mean free path of K^+ -mesons at normal nuclear density ρ_0 is as large as ~ 6 fm. In a previous publication [3] we have shown that the low momentum part of the K^+ -spectrum is sensitive to the in-medium Coulomb and nuclear potential of the kaons, both of which are repulsive. In Sect. 3.2 we compare the data from ANKE (currently the only device where sufficiently small kaon momenta can be measured) with model calculations using a CBUU transport code [4,5]. It is shown that within such a comparison the nuclear K^+ -potential for normal nuclear density can be determined with high accuracy.

Experimental data on the K^+ -production cross section from pn interactions in the close-to-threshold regime are not yet available. This quantity is crucial, for example, for the theoretical description of pA and AA data. Predictions for $R_{np} = \sigma_n/\sigma_p$ range from unity to a factor of six, depending on the underlying model assumptions. In

^a *m.buescher@fz-juelich.de*

Ref. [6] it was proposed that there should be no difference between K^+ production on the neutron and proton, whereas isospin-based models yield $R_{np} \sim 2$ [7] for the total production cross sections. The authors of Ref. [8] draw an analogy between K^+ - and η -meson production and predict $R_{np} \sim 6$. In Sect. 5 we present inclusive ANKE data for K^+ production in pD reactions. Based on a simple phase-space estimate we conclude that the total K^+ -production cross section on neutrons is significantly larger than that on protons.

2 K^+ identification with ANKE and determination of absolute cross sections

2.1 The ANKE spectrometer and K^+ detectors

The COoler SYnchrotron COSY-Jülich [9], which provides proton beams in the range $T_p = 0.04 - 2.83$ GeV, is well suited for the study of K^+ -meson production in pp and pA reactions. In measurements with very thin windowless internal foil or cluster-jet targets, secondary processes involving the produced mesons can be neglected while, at the same time, having sufficiently high luminosities $\mathcal{L} \gtrsim 10^{32} \text{ cm}^{-2}\text{s}^{-1}$ ($\mathcal{L} \gtrsim 10^{31} \text{ cm}^{-2}\text{s}^{-1}$ in case of the cluster-jet target). For the foil-target measurements with ANKE, the proton beam with an intensity of $(2-4) \times 10^{10}$ protons is accelerated to the desired energy on an orbit below the target. These targets are thin triangular-shaped strips of C, Cu, Ag or Au with thicknesses of $(40-1500) \mu\text{g/cm}^2$ [1]. Over a period of approximately 50 s, the beam is slowly steered across the target, keeping the kaon rate in the detectors nearly constant at $(1000-1500) \text{ s}^{-1}$, a level that can be handled by the data acquisition system with dead time corrections of less than 25%. For the study of pD interactions, a deuterium cluster-jet target [10] has been used, providing areal densities of up to $\sim 5 \times 10^{14} \text{ cm}^{-2}$. Due to the lower target density, the cycle times were here typically in the range of 5–30 minutes, and the rate load on the detectors was smaller than in the case of the solid targets.

When using the deuterium cluster-jet target at ANKE, the luminosity can be measured with a telescope consisting of three silicon counters with thicknesses of respectively $60 \mu\text{m}$, $300 \mu\text{m}$, and 5 mm [11]. These so called “spectator” counters are located within the vacuum pipe of the accelerator a few centimetres to the side of the circulating proton beam, see Fig. 1. They cover polar angles in the range $83^\circ - 104^\circ$ and $\pm 7^\circ$ in azimuth. The ability to identify a deuteron and measure its kinetic energy in the telescope allows one to determine the luminosity by measuring proton-deuteron elastic scattering in parallel to kaon production.

Subthreshold K^+ -production was one of the primary motivations for building the large-acceptance ANKE spectrometer [1]. This facility consists of three dipole magnets, which separate forward-emitted reaction products from the circulating proton beam and allow one to determine their emission angles and momenta. Depending

on the choice of the magnetic field in the spectrometer dipole D2 (see Fig. 1), K^+ -mesons in the momentum range $p_K \sim 150 - 600 \text{ MeV/c}$ can be detected. The angular acceptance for these momenta is $\pm 12^\circ$ horizontally and up to $\pm 7^\circ$ vertically.

The layout of ANKE, including detectors and the data-acquisition system, has been optimised to study K^+ spectra at beam energies down to $T_p \sim 1.0$ GeV [2, 12]. This is a very challenging task because of the smallness of the K^+ -production cross sections, *e.g.* 39 nb for pC collisions at 1.0 GeV [13]. The ANKE detection system for K^+ mesons, located along the side of D2, permits kaon identification in a background of pions, protons and scattered particles up to 10^6 times more intense [12]. It consists of two MW-PCs for tracking and momentum reconstruction of ejected tiles produced in the target, as well as for the suppression of background particles scattered by the pole shoes of D2. The 23 TOF-start counters are located close to the exit window of the D2 vacuum chamber in order to maximise the distance to the TOF-stop counters. They are the foremost ones in 15 range telescopes, set up along the focal surface of D2, see Fig. 1. In the telescopes the different ranges of pions, kaons and protons with a given momentum (determined by the width of the telescopes and the dispersion of D2, see also Tables 4 and 5) are utilised for particle identification. Another very effective criterion for K^+ identification is the detection of delayed (with respect to prompt signals from *e.g.* a π^+ produced in the target punching through all counters of a telescope) signals from μ^+ and π^+ in the veto counters. These are produced through the decay of kaons stopped in the ΔE counters or in the second degrader of the same telescope (Fig. 1). For further details of the K^+ identification procedures, we refer to an earlier publication [12]. In the present paper the normalisation of the K^+ yields from the carbon target to pion cross sections from literature and the determination of absolute cross sections is described.

The production of K^+ -mesons has been studied with ANKE at beam energies $T_p = 1.0, 1.2, 1.5, 2.0$ and 2.3 GeV for C, Cu, Ag and Au targets. Two different settings of the magnetic field in D2 were used: $B = 1.3$ T (“1.3 T mode”) for $T_p = 1.0, 1.2, 2.0$ and 2.3 GeV, and $B = 1.57$ T (“1.6 T mode”) for $T_p = 1.2, 1.5$ and 2.3 GeV. With these two modes of operation different regions of the kaon-momentum spectra can be explored. For example, the lower D2 magnetic field of $B = 1.3$ T is sufficient to measure the complete kaon momentum spectrum at $T_p = 1.0$ GeV, whereas with the 1.6 T mode larger kaon momenta are accessible, which is advantageous at higher beam energies. The geometry of the experimental setup as well as the K^+ -identification procedures is identical for the two field values, though different methods for the normalisation to pion cross sections have been applied. The K^+ spectra from pD interactions have been obtained at $T_p = 2.02$ GeV using the 1.6 T mode, and for $T_p = 1.83$ GeV at an intermediate field strength (“1.45 T mode”).

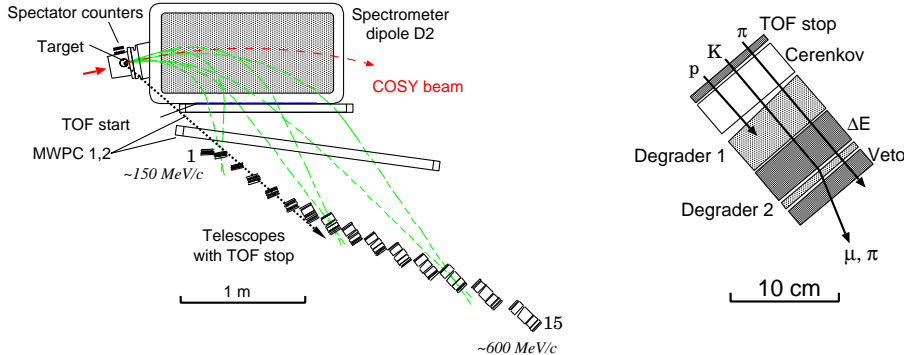


Fig. 1. Layout of ANKE and the K^+ -detection system. The two MWPCs provide tracking and momentum reconstruction of the ejectiles. K^+ -identification is achieved with the help of time-of-flight (TOF) and energy-loss measurements in the 15 range telescopes [12]. The momentum range covered by the telescopes is indicated for the maximum field strength in D2 of $B = 1.57$ T. The dotted line sketches the trajectory of particles bypassing D2 and hitting stop counters 2–5, which are used for luminosity monitoring. Also indicated is the location of the target-near spectator counters for luminosity monitoring together with the cluster target. On the right hand side a schematic top view of one telescope is presented.

2.2 Normalisation of the $pC \rightarrow K^+X$ cross sections

At ANKE absolutely normalised kaon cross sections are deduced from the number of identified kaons $N_{K^+}^i$ in each telescope i (with mean momenta p^i), using differential π^+ cross sections from literature measured under similar kinematical conditions. The detection and identification of π^+ -mesons, which have been measured in different runs with dedicated trigger conditions, in the ANKE detectors is rather simple and the analysis procedures are straightforward. Since the pions can be identified by TOF and energy-loss in the stop counters alone, the pion detection efficiency is given by

$$\epsilon_{\pi^+}^i = \epsilon_{\pi^+}^{\text{TOF}(i)} \cdot \epsilon_{\pi^+}^{\text{MWPC}(i)} \cdot \epsilon_{\pi^+}^{\text{decay}} \quad (1)$$

The efficiency of the TOF- ΔE criterion for pions is large, $\epsilon_{\pi^+}^{\text{TOF}(i)} \geq 98\%$ [12]. The MWPC efficiencies $\epsilon_{\pi^+}^{\text{MWPC}(i)}$ have been measured for each beam energy and are larger than 95%. The decay probabilities between target and stop counters were obtained from simulation calculations.

The differential cross sections for π^+ -production in pC interactions have been taken from Refs. [14, 15]. The π^+ momentum spectrum has been measured at $T_p = 1.0$ GeV for $\vartheta_{\pi^+} = 0^\circ$ at the Petersburg Nuclear Physics Institute (PNPI) [14], whereas at higher beam energies only the production cross sections at a fixed pion momentum of $p_{\pi^+} = 500$ MeV/c and $\vartheta_{\pi^+} = 2.5^\circ$ are known from an experiment at the Lawrence Berkeley Laboratory (LBL) for $T_p = 1.05, 1.73, 2.1, 2.66, 3.5$ and 4.2 GeV [15]. The results of these two experiments have to be combined before they can be used for the normalisation of the ANKE data.

A finer binning of the π^+ cross sections as a function of the beam energy can be achieved when π^- -production cross sections, which have been measured at two intermediate energies, $T_p = 2.66$ and 3.5 GeV [15], are also included into the analysis. The ratio $R = \sigma_{\pi^+}/\sigma_{\pi^-}$ at $p_\pi = 500$ MeV/c as a function of the beam energy T_p is shown in Fig. 2 (upper). When fitting the ratio by a polynomial, only the statistical errors of the data have been

taken into account in order to avoid double counting the systematic errors, which are considered later. The absolute π^- -production cross sections from Ref. [15], can be used to derive the absolute π^+ cross sections at these energies using the ratios from Fig. 2. This gives $d^2\sigma_{\pi^+}/d\Omega dp = (41.8 \pm 1.2)$ and (59.8 ± 1.2) $\mu\text{b}/(\text{sr MeV}/\text{c})$ at $T_p = 2.66$ and 3.5 GeV, respectively.

The combined cross sections for π^+ production are shown in Fig. 2 (middle). In Ref. [14] a total systematic uncertainty of 6% is given, while the authors of Ref. [15] indicate an overall systematic uncertainty of 20% and a relative systematic uncertainty between the individual data points of $\sim 10\%$. The mean value of the PNPI and LBL cross sections at $T_p = 1.0$ GeV of (76.9 ± 4.6) $\mu\text{b}/(\text{sr MeV}/\text{c})$ shown in Fig. 2 (lower) has been calculated according to the averaging method from PDG [17] for results of different experiments. The cross sections from Ref. [15] for $T_p = 1.05, 1.73, 2.1, 2.66, 3.5$ and 4.2 GeV have been scaled up in order to match the averaged value at $T_p = 1.0$ GeV (Fig. 2 (lower)). The individual overall systematic and statistic uncertainties have been added quadratically. The total error of these points then is the product of the above mentioned relative systematic uncertainty in the error of the scaling factor.

In order to determine the π^+ cross section at any intermediate energy, the data have been fitted by a second-order polynomial. The error of the fit has to take into account a complete error matrix since the systematic uncertainties of the data are the main source of the errors. The result of this fitting procedure is presented in Fig. 2 (lower) and Table 1.

In the following the notation $\sigma \equiv d^2\sigma/(d\Omega dp)$ is used for the differential kaon (pion) cross sections which can be calculated from $N_{K^+}^i$ ($N_{\pi^+}^i$) as

$$\sigma_{K^+}(T_p, p^i) = \frac{N_{K^+}^i(T_p)}{(\Delta p \Delta \Omega)_{K^+}^i} \cdot \frac{1}{\mathcal{L}_{K^+}(T_p)} \cdot \frac{1}{\epsilon_{K^+}^i} \quad (2)$$

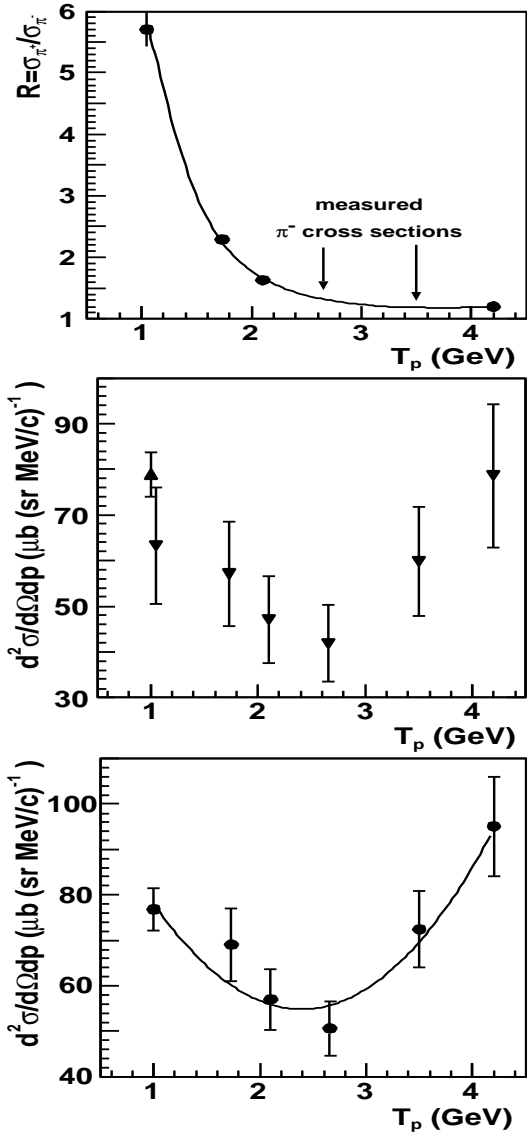


Fig. 2. Upper: Ratio of pion-production cross sections $R = \sigma_{\pi^+}/\sigma_{\pi^-}$ for $pC \rightarrow \pi^\pm X$ reactions at $p_\pi = 500$ MeV/c as a function of the beam energy. The data have been taken from Ref. [15]. Middle: π^+ -production cross sections at $p_\pi = 500$ MeV/c. Upwards pointing triangles denote the data from Ref. [14], downwards represent the data from Ref. [15]. Lower: Averaged π^+ -production cross sections as a function of beam energy. The curve shows the result of the fit with second order polynomial. See text for definition of the error bars.

$$\sigma_{\pi^+}(T_p, p^i) = \frac{N_{\pi^+}^i(T_p)}{(\Delta p \Delta \Omega)_{\pi^+}^i} \cdot \frac{1}{\mathcal{L}_{\pi^+}(T_p)} \cdot \frac{1}{\epsilon_{\pi^+}^i}, \quad (3)$$

where $(\Delta p \Delta \Omega)^i$ are the angular-momentum bins covered by each telescope and \mathcal{L}_{K^+} (\mathcal{L}_{π^+}) denote the luminosities integrated over the corresponding data-taking runs. Similar to pions the kaon-identification efficiencies are given by

$$\epsilon_{K^+}^i = \epsilon_{K^+}^{\text{Tel.}(i)} \cdot \epsilon_{K^+}^{\text{MWPC}(i)} \cdot \epsilon_{K^+}^{\text{decay}}. \quad (4)$$

Table 1. π^+ -production cross sections for $p_{\pi^+} = 500$ MeV/c as a function of the beam energy calculated from the data in Refs. [14, 15]. The errors include all statistical and systematic errors, as explained in the text.

T_p (GeV)	$\frac{d^2\sigma}{d\Omega dp}$ ($\frac{\mu\text{b}}{\text{sr MeV}/c}$)
1.0	78.1 ± 4.6
1.2	71.9 ± 3.9
1.5	64.4 ± 3.5
2.0	56.7 ± 4.0
2.3	55.0 ± 4.2

The efficiencies of the individual telescopes are in the range $\epsilon_{K^+}^{\text{Tel.}(i)} \sim 10 - 30\%$. They have been obtained from a dedicated calibration run at $T_p = 2.3$ GeV [12]. The MWPC efficiencies amount to $\epsilon_{K^+}^{\text{MWPC}(i)} = 71 - 93\%$ [16] depending on the kaon momenta, *i.e.* the telescope number i .

From the analysis outlined above the pion cross sections $\sigma_{\pi^+}(T_p, p^i)$ are available either as $\sigma_{\pi^+}(1.0 \text{ GeV}, p^i)$ (spectra from Ref. [14] downsampled in order to match the average cross section at 1.0 GeV from Table 1) or as $\sigma_{\pi^+}(T_p, 500 \text{ MeV}/c)$ (values given in Table 1). As a consequence, two different normalisation methods have to be used for the two data sets (1.3 and 1.6 T modes): the 1.3 T data comprise the measurement at $T_p = 1.0$ GeV where the pion momentum spectrum is available in the full ANKE momentum range, whereas the 1.6 T data have been obtained at energies $T_p \geq 1.2$ GeV where only the cross sections at $p_{\pi^+} = 500$ MeV/c are known.

Normalisation of the 1.3 T data: The pion and kaon data have been obtained at identical settings of the spectrometer, thus $(\Delta p \Delta \Omega)_{K^+}^i = (\Delta p \Delta \Omega)_{\pi^+}^i$. These angular-momentum bins can be calculated from Eq. (3):

$$(\Delta p \Delta \Omega)^i = \frac{N_{\pi^+}^i(T_p)}{\sigma_{\pi^+}(T_p, p^i)} \cdot \frac{1}{\mathcal{L}_{\pi^+}(T_p)} \cdot \frac{1}{\epsilon_{\pi^+}^i} \\ = \frac{N_{\pi^+}^i(1.0)}{\sigma_{\pi^+}(1.0, p^i)} \cdot \frac{1}{\mathcal{L}_{\pi^+}(1.0)} \cdot \frac{1}{\epsilon_{\pi^+}^i}. \quad (5)$$

Using Eq. (2) one obtains:

$$\sigma_{K^+}(T_p, p^i) = N_{K^+}^i(T_p) \cdot \frac{\sigma_{\pi^+}(1.0, p^i)}{N_{\pi^+}^i(1.0)} \cdot \frac{\mathcal{L}_{\pi^+}(1.0)}{\mathcal{L}_{K^+}(T_p)} \cdot \frac{\epsilon_{\pi^+}^i}{\epsilon_{K^+}^i}. \quad (6)$$

The relative luminosity normalisation $\mathcal{L}_{\pi^+}/\mathcal{L}_{K^+}(T_p)$ has been obtained individually *for each beam energy* by monitoring the interaction of the proton beam with the target to an accuracy of 2% using stop counters 2–5 in four-fold coincidence. This selects ejectiles which are produced in the target by hadronic interactions and bypass the spectrometer dipole D2. The signal of these monitors has been corrected for the dead time of the data acquisition system. For the more general case of different beam energies, *i.e.* for the ratio $\mathcal{L}_{\pi^+}(1.0)/\mathcal{L}_{K^+}(T_p)$ in Eq. (6),

one has to use

$$\begin{aligned} \frac{\mathcal{L}_{\pi^+}(1.0)}{\mathcal{L}_{K^+}(T_p)} &\equiv \frac{\mathcal{L}_{\pi^+}}{\mathcal{L}_{K^+}}(T_p) \cdot \frac{\mathcal{L}_{\pi^+}(1.0)}{\mathcal{L}_{\pi^+}(T_p)} \\ &= \frac{\mathcal{L}_{\pi^+}}{\mathcal{L}_{K^+}}(T_p) \cdot \frac{\sigma_{\pi^+}(T_p, p^i)}{\sigma_{\pi^+}(1.0, p^i)} \cdot \frac{N_{\pi^+}^i(1.0)}{N_{\pi^+}^i(T_p)} . \quad (7) \end{aligned}$$

Since Eq. (7) is valid for any telescope i (*i.e.* momentum p) we choose $i = 15$ since $\sigma_{\pi^+}(T_p, p^i)$ is only available for $p^{i=15} = 500$ MeV/c:

$$\frac{\mathcal{L}_{\pi^+}(1.0)}{\mathcal{L}_{K^+}(T_p)} = \frac{\mathcal{L}_{\pi^+}}{\mathcal{L}_{K^+}}(T_p) \cdot \frac{\sigma_{\pi^+}(T_p, 500)}{\sigma_{\pi^+}(1.0, 500)} \cdot \frac{N_{\pi^+}^{15}(1.0)}{N_{\pi^+}^{15}(T_p)} . \quad (8)$$

Combining Eqs. (6) and (8) one finds the final formula for normalisation of the kaon cross sections:

$$\begin{aligned} \sigma_{K^+}(T_p, p^i) &= N_{K^+}^i(T_p) \cdot \\ &\frac{\sigma_{\pi^+}(1.0, p^i)}{N_{\pi^+}^i(1.0)} \cdot \frac{\mathcal{L}_{\pi^+}}{\mathcal{L}_{K^+}}(T_p) \cdot \frac{\sigma_{\pi^+}(T_p, 500)}{\sigma_{\pi^+}(1.0, 500)} \cdot \frac{N_{\pi^+}^{15}(1.0)}{N_{\pi^+}^{15}(T_p)} \cdot \frac{\epsilon_{\pi^+}^i}{\epsilon_{K^+}^i} . \end{aligned}$$

Normalisation of the 1.6 T data: For the higher field strength the spectra could not be measured at $T_p = 1.0$ GeV, since this energy would result in a too large beam deflection angle in the ANKE dipoles [1]. Hence, Eq. (5) cannot be used and the 1.6 T data have been analysed applying identical cuts such that $(\Delta p \Delta \Omega)^i$ is constant (with an accuracy of better than 5%) for all telescopes and beam energies. Emission angles of the analysed particles $|\theta_{\text{hor}}| < 6^\circ$ and $|\vartheta_{\text{vert}}| < 3.5^\circ$ have been selected, the momentum acceptance of each telescope has been restricted to $\Delta p < 6$ MeV/c. In the 1.6 T mode particles with $p = 500$ MeV/c are detected in telescope 13, thus:

$$\begin{aligned} (\Delta p \Delta \Omega)^i &= (\Delta p \Delta \Omega)^{13} = \\ &\frac{N_{\pi^+}^{13}(T_p)}{\sigma_{\pi^+}(T_p, 500)} \cdot \frac{1}{\mathcal{L}_{\pi^+}(T_p)} \cdot \frac{1}{\epsilon_{\pi^+}^{13}} . \quad (9) \end{aligned}$$

Together with Eq. (2) this leads to:

$$\begin{aligned} \sigma_{K^+}(T_p, p_i) &= N_{K^+}^i(T_p) \cdot \\ &\frac{\sigma_{\pi^+}(T_p, 500)}{N_{\pi^+}^{13}(T_p)} \cdot \frac{\mathcal{L}_{\pi^+}}{\mathcal{L}_{K^+}}(T_p) \cdot \frac{\epsilon_{\pi^+}^{13}}{\epsilon_{K^+}^i} . \quad (10) \end{aligned}$$

In principle, the (simpler) 1.6 T normalisation formula could also be applied to the 1.3 T data. However, the latter were generally measured with lower statistics which would be further reduced by the restriction of the accepted angles $\Delta\Omega$ and momenta Δp leading to significantly larger statistical uncertainties.

2.3 Target-mass dependence of the cross sections

The target-mass dependence of the K^+ -production cross sections has been determined using the formula:

$$R(A/C) \equiv \frac{\sigma_{K^+}^A(p^i)}{\sigma_{K^+}^C(p^i)} = \left[\frac{N_{K^+}^A}{N_{K^+}^C} \right]_{\text{tel.}(i)} \cdot \frac{\mathcal{L}^C}{\mathcal{L}^A} . \quad (11)$$

Here the index “ A ” stands for the copper, silver and gold targets, respectively, while “ C ” refers to carbon. N_{K^+} is the number of identified kaons in each telescope i after dead-time corrections. \mathcal{L} stands for the integrated luminosity during data taking for the particular target.

In principle, absolute production cross sections could have been determined also for the heavier targets using the normalisation procedure described in the previous paragraph. However, absolute cross sections for Cu, Ag and Au are not needed for the following analyses, but only the cross-section ratios $\sigma_{K^+}^A/\sigma_{K^+}^C$. These have the advantage of higher accuracy since many possible systematic errors, such as corrections for the detection efficiencies in the ANKE range telescopes, cancel out.

The luminosity ratio $\mathcal{L}^C/\mathcal{L}^A$ in Eq. (11) can be deduced from the ratio of pion rates, measured under identical experimental conditions for each target during calibration runs using an on-line trigger optimised for π^+ detection:

$$\frac{\mathcal{L}^C}{\mathcal{L}^A} = \left[\frac{N_{\pi^+}^C}{N_{\pi^+}^A} \right]_{\text{tel.}\#13/15} \cdot \left[\frac{\sigma_{\pi^+}^A}{\sigma_{\pi^+}^C} \right]_{p=500 \text{ MeV/c}} . \quad (12)$$

N_{π^+} is the number of pions detected by telescope #13 (which detects ejectiles with momenta of 500 MeV/c in the 1.6 T mode) or #15 (1.3 T mode), normalised to the proton-beam flux. For a momentum of 500 MeV/c the ratio of the pion-production cross sections σ_{π^+} can be extracted from experimental data [14, 15, 18] taken in the energy range $T_p = 0.73 - 4.2$ GeV at emission angles of 0° , 2.5° and 15° . Figure 3 shows the cross-section ratios for Cu/C and Pb/C calculated from those data.

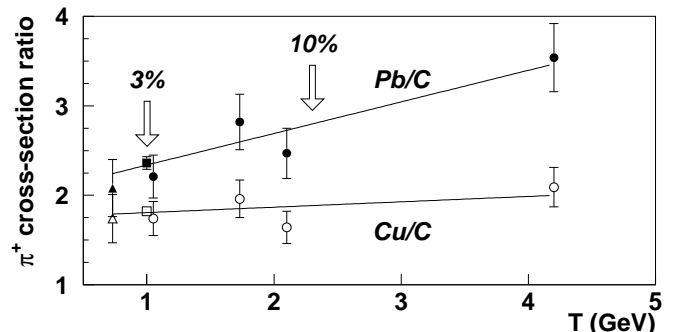


Fig. 3. Ratios of the π^+ -production cross sections for Cu/C and Pb/C at $p_{\pi^+} = 500$ MeV/c as a function of the projectile energy T_p . The data were taken from Refs. [18] (triangles, $T_p = 0.73$ GeV, $\vartheta_{\pi^+} = 15^\circ$), [14] (squares, $T_p = 1.0$ GeV, $\vartheta_{\pi^+} = 0^\circ$) and [15] (circles, $T_p = 1.05 - 4.2$ GeV, $\vartheta_{\pi^+} = 2.5^\circ$). The lines are linear fits to the data points. The arrows indicate the uncertainties of the ratios at the minimum and maximum energy measured with ANKE.

From Fig. 3 one can deduce the π^+ -production ratios for Cu/C and Au/C. For Cu/C values of 1.81 ± 0.05 at $T_p = 1.0$ GeV and 1.88 ± 0.18 at $T_p = 2.3$ GeV are obtained. For Pb/C the ratios are 2.34 ± 0.07 and 2.80 ± 0.29 ,

respectively. All values agree within 10% with ratios scaling as $A^{1/3}$, *i.e.* 1.74 and 2.58 for Cu/C and Pb/C, respectively. Thus, assuming an $A^{1/3}$ dependence, it is possible to calculate from the ratios Pb/C those for Au/C. We use for the ratio Au/C values of 2.29 ± 0.07 at $T_p = 1.0$ GeV and 2.73 ± 0.27 at $T_p = 2.3$ GeV. The analysis of our π^+ -data shows that the cross-section ratios are to about 2% independent of the π^+ -emission angle within the ANKE angular acceptance.

3 Inclusive K^+ -momentum spectra for $A \geq 12$

3.1 Absolute cross sections for $p^{12}\text{C} \rightarrow K^+ X$ reactions

The measured cross sections for K^+ production in $p\text{C}$ interactions are shown in Fig. 4 and listed in Tables 4 and 5. The overall systematic uncertainties coming from the normalisation to pion data described in Sect. 2.2 (*i.e.* errors given in the right column of Table 1 plus 2% for the uncertainty of the beam monitoring) are $\epsilon_{\text{syst}} = 8, 7, 7, 9$ and 10% for $T_p = 1.0, 1.2, 1.5, 2.0$ and 2.3 GeV, respectively. The error bars of the individual data points include the uncertainties arising from the efficiency-correction factors of Eq. (1) and (4) but not the overall uncertainty from the pion normalisation. In both operation modes of D2, kaons could be identified in telescopes #3–15 whereas in the two closest telescopes the background from scattered particles turned out to be too large.

At $T_p = 2.3$ GeV there are discrepancies between the two data sets for $p_{K^+} \leq 450$ MeV/c, whereas at $T_p = 1.2$ GeV they coincide. This cannot be caused by the angular dependence of K^+ production because the cross sections evaluated in the even more restricted angular interval, $|\theta_{\text{hor}}| < 4^\circ$ and $|\vartheta_{\text{vert}}| < 2.5^\circ$ are in agreement with those obtained for $|\theta_{\text{hor}}| < 6^\circ$ and $|\vartheta_{\text{vert}}| < 3.5^\circ$. Furthermore, the discrepancy is unlikely to be due to the K^+ identification procedure since, for this particular energy, different analysis algorithms were applied giving a difference in the cross sections smaller than 2%. We conclude that there is an unknown source of systematic errors, which may yield an additional uncertainty of up to 30% at the highest measured beam energy. These uncertainties vanish when one calculates the cross-section ratios for different target nuclei.

3.2 Target-mass dependence

The cross section ratios $R(A/\text{C})$, measured with the two operation modes of D2, for beam energies $T_p = 1.0, 1.5, 1.75$ and 2.3 GeV are listed in Tables 6, 7, 8 and 9. These complement the published partial results [2,3]. No data for targets heavier than carbon was taken for $T_p = 1.2$ and 2.0 GeV, whereas the absolute normalisation was not established at $T_p = 1.75$ GeV.

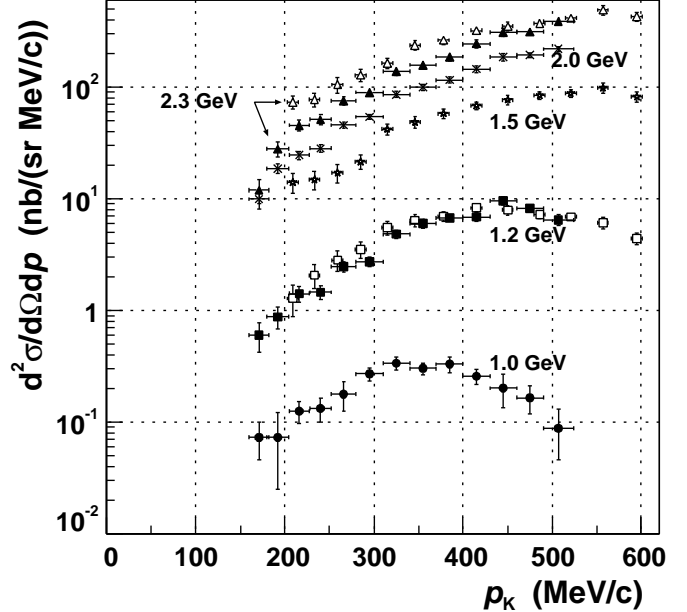


Fig. 4. Double differential $p^{12}\text{C} \rightarrow K^+ X$ cross sections measured at ANKE, the numerical values being given in Tables 4 and 5. Black circles denote the cross sections measured at $T_p = 1.0$ GeV [2], squares at $T_p = 1.2$ GeV, stars at $T_p = 1.5$ GeV, crosses at $T_p = 2.0$ GeV and triangles at $T_p = 2.3$ GeV. Closed symbols correspond to the measurements with $B = 1.3$ T in the full ANKE acceptance, while open symbols to $B = 1.57$ T and $\theta_{\text{hor}} < 6^\circ$, $\vartheta_{\text{vert}} < 3.5^\circ$. The error bars do not include the systematic uncertainties from the normalisation to pion data.

The measured ratios $R(\text{Au/C})$ at all beam energies are shown in Fig. 5. For $T_p \geq 1.5$ GeV all data exhibit similar shapes, rising steadily with decreasing kaon momenta, passing a maximum and falling steeply at low momenta. The maxima around $p_{\text{max}} \sim 245$ MeV/c coincide within 2 MeV/c, *i.e.* their positions do not depend on the proton beam energy. The peak structure seems not to be visible at $T_p = 1.0$ GeV. However, at this low beam energy the large background only permitted us to extract the cross sections for the heavy targets down to $p_K \sim 220$ MeV/c, which is only slightly below the peak positions observed at $T_p \geq 1.5$ GeV. Given the large error bars, the 1.0 GeV data are not in disagreement with the strong decrease observed at higher energies. The independence of the peak positions from the beam energy T_p suggests that the effect is due to FSI effects of the produced kaons, since the basic production mechanism may change from 1.5 to 2.3 GeV, see Sect. 4.

For higher kaon momenta the ratios $R(\text{Au/C})$ decrease with T_p , possibly reflecting changes of the production mechanisms with beam energy. To ensure that the pronounced peak structure of $R(\text{Au/C})$ is not an artefact of the ANKE detection system, the 2.3 GeV data were taken with both operation modes of D2, resulting in a change in the values of the momenta that are focused onto the individual range telescopes [12]. The data from Table 9 for $R(\text{Au/C})$ at $T_p = 2.3$ GeV obtained with the 1.3 T and 1.6 T

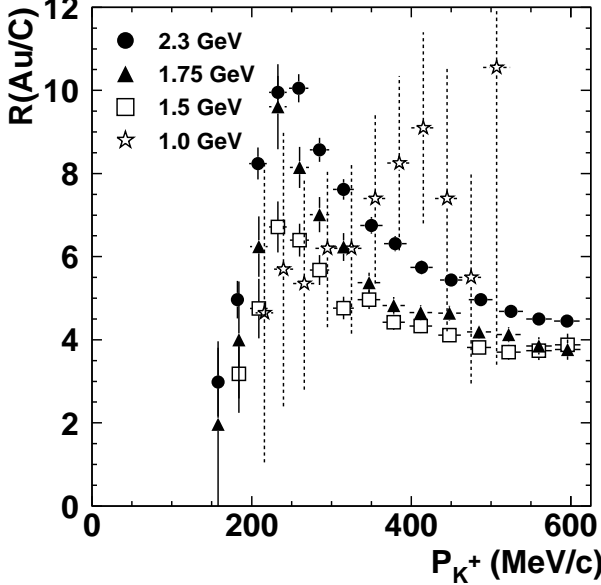


Fig. 5. Ratios of the K^+ -production cross sections $R(Au/C)$ measured at $T_p = 1.0, 1.5, 1.75$ and 2.3 GeV as a function of the laboratory kaon momentum p_{K^+} (cf. Tables 6 – 9).

modes, show that these data sets agree, as illustrated in Fig. 6 for $R(Au/C)$. This also demonstrates that the 30% uncertainty of the absolute cross sections measured at $T_p = 2.3$ GeV cancels out for the ratios. In addition, the statistical errors are significantly smaller here. Consistent values for the ratios were also obtained when the polar K^+ -emission angles were restricted to $\vartheta_{K^+} < 3^\circ$, as shown in Fig. 6.

The ratios of kaon-production cross sections $R(Cu/C)$, $R(Ag/C)$ and $R(Au/C)$ measured at 2.3 GeV are presented in Fig. 7. The position of the maximum of $R(A/C)$ varies with nucleus; a fit to the data results in $p_{\max} = 211 \pm 6$, 232 ± 6 and 245 ± 5 MeV/c for Cu, Ag and Au, respectively [3].

In an earlier publication [3] we showed that from the cross section ratios $R(A/C)$ the nuclear K^+ -potential for normal nuclear density can be derived with high accuracy. This is illustrated in Fig. 7, where the results of model calculations for $R(Au/C)$ within the CBUU transport code [4, 5] are plotted. Without any FSI the ratio $R(Au/C)$ is almost independent of the kaon momentum, and the average ratio $R(Au/C) \sim 9$ corresponds to an A -dependence $\sigma \propto A^\alpha$ with $\alpha \sim 0.79$. A detailed discussion of the relation between α and the different mechanisms leading to K^+ -production in nuclei can be found in an Ref. [19].

Rescattering processes tend to slow down the produced kaons leading to a steadily rising ratio with decreasing K^+ -momenta. In a purely classical picture, kaons produced at some radius R in a nucleus acquire an additional momentum of $p_{\min} = \sqrt{2m_K V_C(R)}$ in the repul-

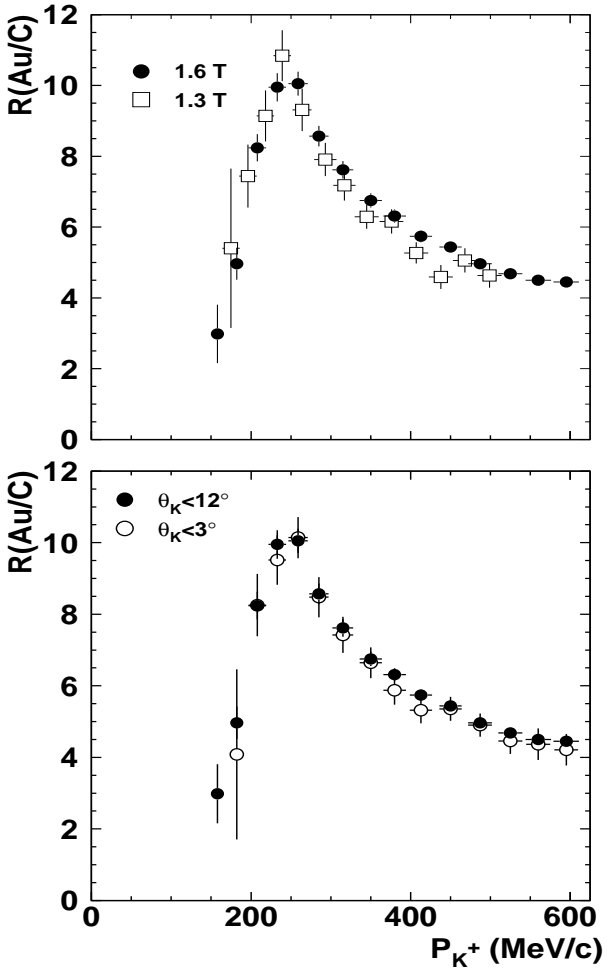


Fig. 6. Upper: Ratios of the K^+ -production cross sections $R(Au/C)$ measured at $T_p = 2.3$ GeV and different operation modes of D2 (cf. Table 9). Lower: Same ratios measured in the full ANKE acceptance and restricted to angles $\vartheta_{K^+} < 3^\circ$.

sive Coulomb potential. This corresponds to a minimum momentum of $p_K \sim 130$ MeV/c for an Au nucleus. Thus $R(Au/C)$ should drop to zero for smaller kaon momenta. This is well reproduced by the calculations presented in Fig. 7 and results in the pronounced peak structure of the cross-section ratios. From this peak position, which can be determined with high accuracy both in the data and the calculated spectra, the nuclear K^+ -potential can be determined with high accuracy [3].

The repulsive nuclear K^+ -potential, which is expected to be of strength $V_K = 22 \pm 5$ MeV [20], independent of the target mass A , shifts the kaon momenta, and thus the peak positions, to higher values. In Fig. 7 we illustrate this effect for $V_K = 0, 20$ and 40 MeV. The best agreement between the measured and calculated peak positions is obtained for $V_K = 20$ MeV with an estimated uncertainty of about ± 3 MeV. We expect that an even higher precision could be obtained from refined model calculations for the full data set (all beam energies and target nuclei) which not only reproduce the peak positions of $R(A/C)$ but also the

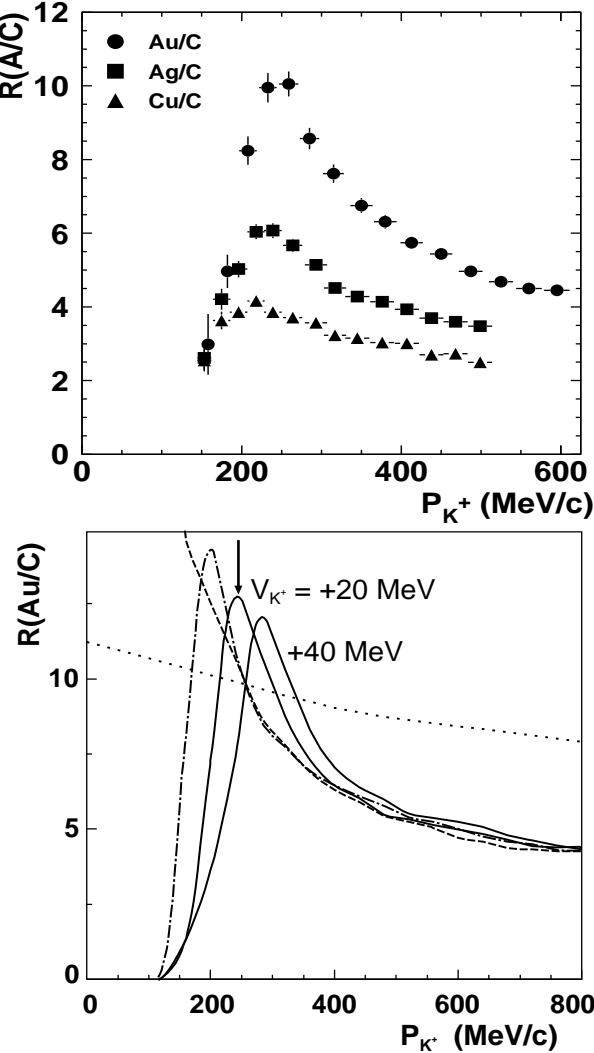


Fig. 7. Upper: Ratios of the K^+ -production cross sections $R(\text{Cu/C})$ (1.3 T), $R(\text{Ag/C})$ (1.3 T), $R(\text{Au/C})$ (1.6 T) measured at $T_p = 2.3$ GeV as a function of the laboratory kaon momentum (cf. Table 9). Lower: Result of model calculations with the CBUU transport code [5] for $R(\text{Au/C})$ showing the effect of K^+ rescattering, the Coulomb and nuclear K^+ potentials (dotted line: no rescattering and no potentials; dashed: only rescattering, no potentials; dashed-dotted: rescattering plus Coulomb; solid: full calculation taking into account rescattering, Coulomb and different nuclear potentials). The arrow indicates the position of the maximum of the measured ratio $R(\text{Au/C})$.

shape of all measured distributions, in particular at low kaon momenta [21].

4 Systematics of available p C cross sections

Table 2 lists the available data on K^+ -production in pA collisions from ANKE and elsewhere in the literature. The different data sets were obtained for non-overlapping kinematical parameters (*i.e.* beam energies, kaon emission an-

gles and momenta) which prevents a direct comparison with the results from ANKE and, *e.g.*, a test of the overall normalisations.

In Ref. [19] it was shown that the measured invariant cross sections $E d^3\sigma/d^3p$ follow an exponential scaling behavior when plotted as a function of the four-momentum transfer t , as illustrated in Fig. 8.

Apart from the data taken with ANKE at $T_p = 1.0$ and 1.2 GeV, all spectra cover the range of negative t . The sharp fall-off of the cross sections from ANKE towards positive values of t was explained in Ref. [19] by the fact that the data were taken very close to the kinematical limit for hypernucleus formation at $t = 0.145$ GeV 2 ($T_p = 1.0$ GeV) which is usually accompanied by very small cross sections. It can also be an indication for a change of the kaon production mechanism. For $t < 0$ the individual data sets show exponential dependences of the form $E d^3\sigma/d^3p = c_0 \exp[b_0 t]$, with parameters c_0 and b_0 being given in Ref. [19]. It has been speculated that the differing slope parameters, as well as deviations from the exponential behaviour (see, *e.g.*, the data from KaoS [27] in Fig. 8), reflect a dependence on the available squared CM energy s and the excitation energy of the target nucleus, $\Delta m = m_X - m_A$, where m_X and m_A denote the masses of the target nucleus before and after the reaction process, respectively [19]. Based on Regge phenomenology the following formula has been suggested as a parameterisation of the invariant cross section:

$$E \frac{d^3\sigma}{d^3p} \propto f(t, m_X^2) \exp[b_0 t \cdot \ln(s/s_0)]. \quad (13)$$

Figure 8 shows the invariant cross sections, divided by an average s, t dependence using $b_0 = 2.2$ GeV $^{-2}$ (indicated by the dashed line in Fig. 8) and $s_0 = 100$ GeV 2 , as a function of the excitation energy Δm . The solid lines in Fig. 8 correspond to a parameterisation of the invariant cross sections in $p^{12}\text{C}$ interactions

$$\begin{aligned} E \frac{d^3\sigma}{d^3p} &= \sigma_0 \cdot \Delta m^{N_0} \cdot \exp[b_0 t \cdot \ln(s/s_0)] \\ &= \sigma_0 \cdot \Delta m^{N_0} \cdot (s/s_0)^{b_0 t}, \end{aligned} \quad (14)$$

with fitted parameters as summarised in Table 3.

Table 3. Parameters obtained from a fit with Eq. (14)

T_p (GeV)	σ_0 (nb GeV $^{-2}$ c 3 sr $^{-1}$)	N_0 (n)	b_0 (GeV $^{-2}$)	s_0 (GeV 2)
<1.58	25	17 (13)	2.2	100
>1.58	1000	9.5 (8)		

The term Δm^{N_0} reflects a phase space behaviour $\sigma \propto \Delta m^{N_0} = \Delta m^{(3n-5)/2}$ with n particles in the final state. As can be seen from Fig. 8, the parameterization from

Table 2. Data on K^+ -production in pA collisions (ordered by the year of publication) at various beam energies T_p , kaon momenta p_K and emission angles ϑ_K .

T_p (GeV)	Targets	p_K (MeV/c)	ϑ_K ($^\circ$)	Measured at
0.842 - 0.99	Be...Pb	<i>total cross sections</i>		PNPI [13]
2.1	NaF, Pb	350–750	15–80	LBL [22]
1.2, 1.5, 2.5	C, Pb	500–700	40	SATURNE [23]
1.2	C	165–255	90	CELSIUS [24]
1.7 - 2.91	Be	1280	10.5	ITEP [25]
2.9	Be	545	17	ITEP [26]
1.0	C, Cu, Au	171–507	≤ 12	ANKE [2]
1.6	C, Au	275–1075	40–64	KaoS [27]
1.6	Ni	275–1075	40	KaoS [27]
2.5, 3.5	C, Au	275–1075	32–64	KaoS [27]
2.5, 3.5	Ni	275–1075	40	KaoS [27]
1.0, 1.2, 1.5, 2.0, 2.3	C,Cu,Ag,Au	171–595	≤ 12	ANKE

Eq. (14) can describe all available data on K^+ -production in pA reactions obtained in largely different angular-momentum intervals within a factor $\sim 2 - 3$. Within this uncertainty the cross sections from ANKE are in agreement with those from other experiments.

The parameterisation given by Eq. (14) not only supplies a Lorentz-invariant description of all available data which is independent of the choice of the reference system, pp or pA . Fig. 8 also reveals that:

1. The 1.0 GeV ANKE data were obtained down to $\Delta m = 1.173 \text{ GeV/c}^2$, *i.e.* very close to the kinematical limit at $\Delta m_{\min} = m_A = 1.116 \text{ GeV/c}^2$. In this limiting case no energy can be transferred to excite the target nucleus or knock out target nucleons. The target nucleus must take part in the reaction as a whole such that the effective target mass is $12 \cdot m_N$. There are only two particles, K^+ -meson and nucleus, in the final state ($n = 2$).
2. Within a phase-space treatment of the final state, the steep rise ($N_0 = 17$, $n = 13$) of the subthreshold data indicates that all 12 nucleons plus the Λ -hyperon carry away energy in the final state. This seems to be in contradiction with the above statement of $n = 2$. However, it might reflect the fact that more and more nucleons in the *initial state* must take part in the kaon-production process when approaching the kinematical limit. In fact, the data at 1.0 GeV, far below the free nucleon-nucleon threshold at $T_{NN} = 1.58 \text{ GeV}$, reveal a high degree of collectivity in the target nucleus (see Ref. [2]). For example, if the kaons are produced in a collision of the 1.0 GeV beam proton with a single target nucleon, internal momenta of at least $\sim 550 \text{ MeV/c}$ are needed in order to produce kaons in the forward direction with momenta of $p_{K^+} \sim 500 \text{ MeV/c}$ (the highest kaon momenta measured at this beam energy). Such high momentum components are essentially due to many-body correlations in the nucleus. Within a very simple phase-space approximation (which neglects the intrinsic motion of the target nucleons) it can be shown that the number of participating target nucleons must be

$\sim 5 - 6$. It has been suggested [5,13,28–32] that such effects can be described in terms of multi-step mechanisms or high-momentum components in the nuclear wave function.

3. The different slope parameters N_0 below and above the free NN threshold ($T_{NN} = 1.58 \text{ GeV}$) indicates a change of the K^+ -production mechanism. This has been proposed long ago in Ref. [13] and is confirmed by microscopical model calculations [5,28–32] and recent K^+d coincidence measurements with ANKE [33]. These suggest that below threshold the kaons are dominantly produced in two-step reactions with intermediate pion formation, whereas at higher energies direct K^+ production on a single nucleon prevails.

5 Inclusive K^+ cross sections from pD interactions

K^+ -production in pD interactions was measured at two beam energies, $T_p = 1.83$ and 2.02 GeV . ANKE was operated in the 1.45 T and 1.6 T modes and the vertical and horizontal kaon emission angles were restricted to $\vartheta < 4^\circ$ during data analysis. For absolute normalisation of the cross sections the luminosity \mathcal{L} has been determined with the help of pd elastically scattered events. These have been measured with the ANKE spectator-detection system; details of the detectors and the normalisation procedure are described in Ref. [11]. The overall systematic uncertainty in the absolute normalisation is 20%. All other analysis procedures are in accord with those for the heavier targets described in Sect. 2.1.

Figure 9 shows the K^+ -momentum spectra measured at beam energies $T_p = 1.83 \text{ GeV}$ and at 2.02 GeV on the deuteron target in comparison with the one for carbon at 2.0 GeV . The difference between the pD cross sections can be attributed to the fact that the lower energy is significantly closer to the free nucleon-nucleon threshold. The different pD and pC cross sections at $T_p = 2.0 \text{ GeV}$ can be explained in the framework of the Glauber model [34]. In this model, beam protons effectively “sees” 7.3 nucleons

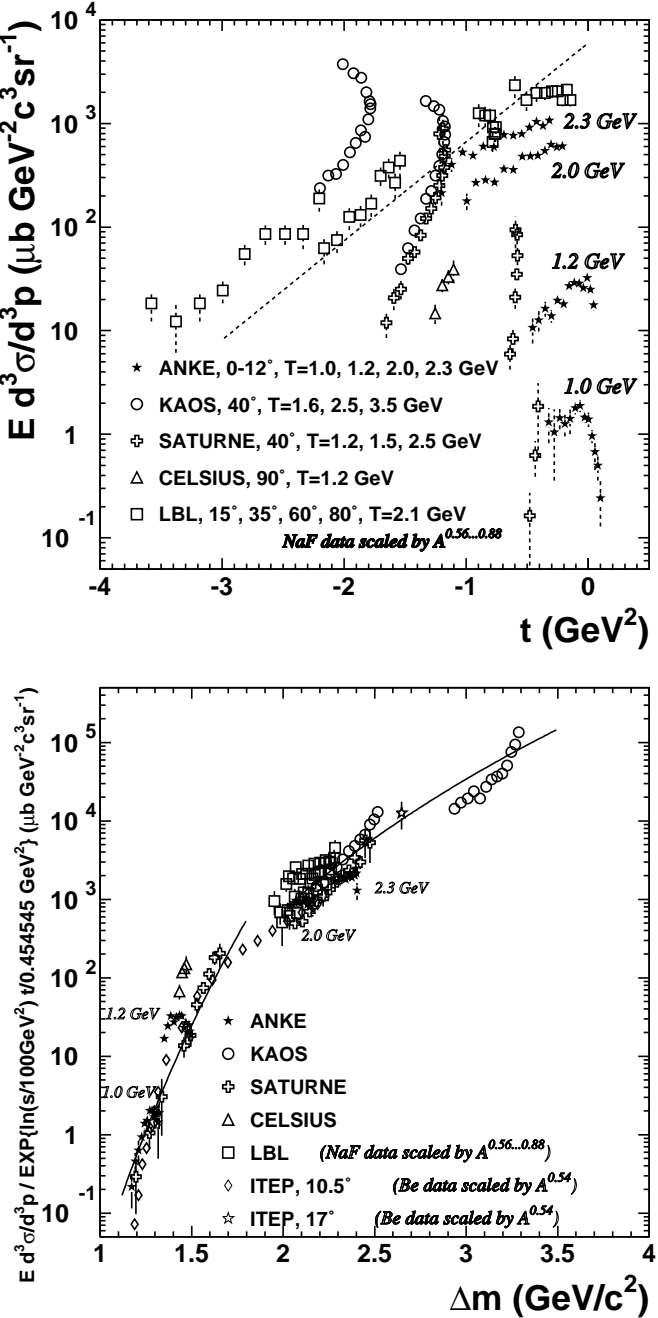


Fig. 8. Upper: Invariant $p^{12}\text{C} \rightarrow K^+X$ cross sections as a function of the four-momentum transfer t between the beam proton and the outgoing kaon. Lower: Scaled invariant $p^{12}\text{C} \rightarrow K^+X$ cross sections as a function of the excitation energy Δm of the target nucleus. The data from LBL [22] and ITEP [25, 26] were measured with NaF (Be) targets and were corrected for the target-mass dependence according to Ref. [19]. The beam energies of the ANKE data sets (filled stars) are indicated; for $T_p = 2.3$ GeV the data obtained with $B = 1.3$ T (closed triangles in Fig. 4) were used.

in a carbon target [5, 13]. Thus the ratio of the $p\text{C}$ and $p\text{D}$ cross sections should be about 3.5, which is confirmed by the data. This finding suggests that at $T_p = 2.0$ GeV kaons are produced on individual nucleons both in deuteron and carbon targets. There is no indication for any collective target behaviour, which is in line with the discussion in Sect. 4. Furthermore, shadowing effects in the deuteron are smaller than 5% [35]. Therefore, for the following analysis, which is carried out in a simple phase-space approach, we assume $\sigma_D = \sigma_p + \sigma_n$, with σ_n/σ_p being a free parameter.

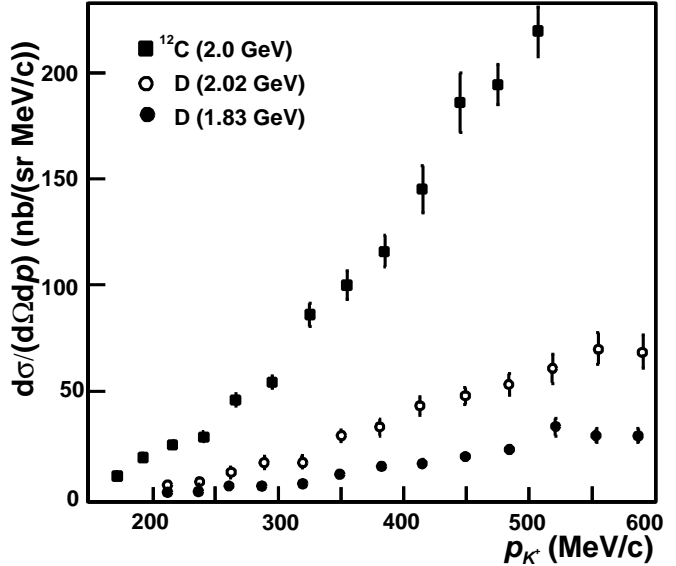


Fig. 9. Double differential cross sections for K^+ production on a deuteron target measured at $T_p = 1.83$ and 2.02 GeV (c.f. Table 10) and on a carbon target at 2.0 GeV (c.f. Table 4).

Following the analysis in Ref. [7] of different inclusive reactions giving rise to K^+ -production, six main reaction channels lead to kaon production on the deuteron at our beam energies. They are listed in Table 11 together with the corresponding cross sections which have been calculated using the parameterisations given in Ref. [7]. The calculated value for $\sigma(pp \rightarrow pK^+\Lambda)$ at 2.0 GeV is in agreement with the experimental result from Ref. [36]. For the simulation of phase-space distributed $p\text{D} \rightarrow K^+X$ events, the PLUTO package [37], which takes into account the intrinsic motion of the nucleons in the deuteron, has been used. The events have been generated for each reaction channel and weighted according to the total cross sections from Table 11. Each event subsequently has been tracked through the spectrometer dipole and all detection efficiencies have been taken into account. A comparison of the simulated spectra with the data is shown in Fig. 10 (curve labelled by “ $\sigma_n = 2\sigma_p$ ”).

The apparent difference between the calculated and measured cross sections can be due to the following reasons: our simple approach does not take into account the dynamics of the interaction in the different states (such as initial- and final-state interactions) and the ratio σ_n/σ_p

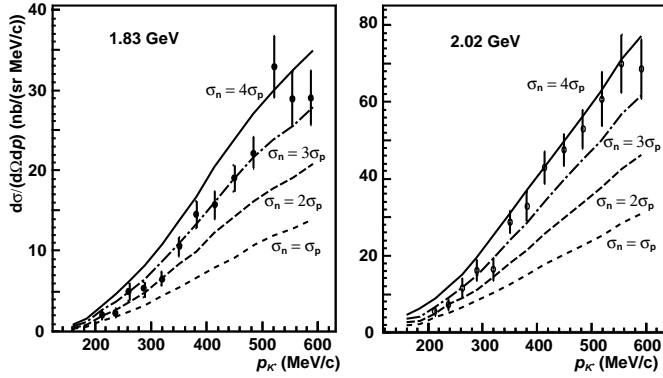


Fig. 10. Double differential $pD \rightarrow K^+X$ cross section at 1.83 GeV and at 2.02 GeV in comparison with our model calculations using different ratios σ_n/σ_p (lines).

might be different from that suggested in Ref. [7]. Thus we repeated the simulations keeping the relative weights of the three pp and pn channels constant (as given in Table 11) while treating the ratio of the sum of these two contributions, *i.e.* σ_n/σ_p , as a free parameter. The result of the simulations with different ratios σ_n/σ_p is also shown in Fig. 10. The best agreement between data and calculations is obtained for $\sigma_n/\sigma_p \sim 3$ at 1.83 GeV and $\sigma_n/\sigma_p \sim 4$ at 2.02 GeV.

6 Summary and outlook

In this paper we present the full set of inclusive data on $pA \rightarrow K^+X$ reactions measured at forward angles with the ANKE spectrometer at COSY-Jülich. Far below the free nucleon-nucleon threshold there must be a strong collective behavior of the target nuclei, whereas a change of the reaction mechanism is observed at higher energies. For a better understanding of the reaction mechanisms further microscopical model calculations should be performed. Such calculations are also needed to extract the precise value of the in-medium nuclear K^+ -potential from the cross-section ratios $R(A/C)$ measured at ANKE.

The cross sections from ANKE are compatible with those obtained at other facilities. All data sets together now cover a wide kinematical range, *i.e.* beam energies, kaon momenta and emission angles. We currently do not foresee further inclusive measurements since we regard the existing data sets — in particular with recent results from the KaoS collaboration obtained at larger kaon-emission angles [27] — as being largely sufficient. However, we expect that significant progress for the understanding of the K^+ -production mechanisms will come from correlation data, where the produced kaons are measured in coincidence with protons, deuterons and other light fragments. A first step in this direction has already been made at ANKE. Data on the reaction $p(1.2\text{ GeV})C \rightarrow K^+dX$ provide the first direct indication for kaon production in the particular two-step reaction $pN_1 \rightarrow \pi d, \pi N_2 \rightarrow K^+\Lambda$ with formation of intermediate pions in the target nucleus [33].

The data also hint on processes involving $p(2N) \rightarrow K^+dA$ reactions on two-nucleon clusters.

First correlation measurements have also been performed using deuteron targets. A preliminary analysis of the proton-momentum spectra from $pD \rightarrow K^+pX$ events confirm our present conclusion from the inclusive data that the K^+ -production cross section on neutrons is significantly larger than on protons [38]. This finding should be taken into account in future model calculations, especially of K^+ production in heavy ion reactions.

It is also planned to measure at ANKE the production of K^+K^- pairs in pA collisions. It can be expected that the measurement of low-momentum kaons offers the unique possibility to determine the nuclear K^- -potential for normal nuclear density with similar accuracy to that of the K^+ -mesons.

Acknowledgments

This work profited significantly from discussions with members of the ANKE collaboration, in particular W. Cassing, A. Sibirtsev and C. Wilkin. We are also grateful to R. Schleichert as the technical coordinator of ANKE and to C. Wilkin for carefully reading the manuscript. Financial support from the following funding agencies was of indispensable help for building ANKE, its detectors and DAQ: Germany (BMBF: grants WTZ-RUS-649-96, WTZ-RUS-666-97, WTZ-RUS-685-99, WTZ-POL-007-99, WTZ-POL-015-01, WTZ-POL-041-01; DFG: 436 RUS 113/337, 436 RUS 113/444, 436 RUS 113/561, State of North-Rhine Westfalia), Poland (Polish State Committee for Scientific Research: 2 P03B 101 19), Russia (Russian Ministry of Science: FNP-125.03, Russian Academy of Science: 99-02-04034, 99-02-18179a) and European Community (INTAS-98-500).

References

1. S. Barsov *et al.*, *Nucl. Instr. Methods Phys. Res., Sect. A* **462**, 364 (2001).
2. V. Koptev *et al.*, *Phys. Rev. Lett.* **87**, 022310 (2001).
3. M. Nekipelov *et al.*, *Phys. Lett. B* **540**, 207 (2002).
4. G. Wolf *et al.*, *Nucl. Phys. A* **552**, 549 (1993).
5. Z. Rudy *et al.*, *Eur. Phys. J. A* **15**, 303 (2002).
6. P.A. Piroué and A. J. S. Smith, *Phys. Rev.* **148**, 1315 (1966).
7. K. Tsushima *et al.*, *Phys. Rev. C* **59**, 369 (1999).
8. G. Fäldt and C. Wilkin, *Z. Phys. A* **357**, 241 (1997).
9. R. Maier, *Nucl. Instr. Methods Phys. Res., Sect. A* **390**, 1 (1997).
10. R. Santo *et al.*, *Nucl. Instr. Methods Phys. Res., Sect. A* **386**, 228 (1997); A. Khoukaz *et al.*, *Eur. Phys. J. D* **5**, 275 (1999).
11. I. Lehmann, Ph.D. thesis, Universität zu Köln (2003); I. Lehmann *et al.*, *Nucl. Instr. Methods Phys. Res., Sect. A* (in preparation).
12. M. Büscher *et al.*, *Nucl. Instr. Methods Phys. Res., Sect. A* **481**, 378 (2002).

13. V. Koptev *et al.*, *JETP* **67**, 2177 (1988).
14. V.V. Abaev *et al.*, *J. Phys. G* **14**, 903 (1988).
15. J. Papp *et al.*, *Phys. Rev. Lett.* **34**, 601 (1975).
16. V. Kleber *et al.*, *Phys. Rev. Lett.* **91**, 172304 (2003).
17. K. Hagiwara *et al.* (Particle Data Group), *Phys. Rev. D* **66**, 010001 (2002).
18. D.R.F. Cochran *et al.*, *Phys. Rev. D* **6**, 3085 (1972).
19. M. Büscher *et al.*, *Phys. Rev. C* **65**, 014603 (2001).
20. A. Sibirtsev and W. Cassing, *Nucl. Phys. A* **641**, 476 (1998).
21. Z. Rudy *et al.*, (in preparation).
22. S. Schnetzer *et al.*, *Phys. Rev. C* **40**, 640 (1989).
23. M. Debowski *et al.*, *Z. Phys. A* **356**, 313 (1996).
24. A. Badalà *et al.*, *Phys. Rev. Lett.* **80**, 4863 (1998).
25. A.V. Akindinov *et al.*, *JETP Lett.* **72**, 100 (2000).
26. M. Büscher *et al.*, *Z. Phys. A* **355**, 93 (1996).
27. W. Scheinast, KaoS Collaboration, Proc. 7th Int. Workshop on Meson Production, Properties and Interaction MESON2002, 24 – 28 May 2002, Cracow, Poland; World Scientific Publishing, ISBN 981-238-160-0, L. Jarczyk, A. Magiera, C. Guaraldo, H. Machner, (editors), p. 493 (2003); and private communication.
28. W. Cassing *et al.*, *Phys. Lett. B* **238**, 25 (1990).
29. H. Müller and K. Sistemich, *Z. Phys. A* **344**, 197 (1992).
30. A.A. Sibirtsev and M. Büscher, *Z. Phys. A* **347**, 191 (1994).
31. E.Ya. Paryev, *Eur. Phys. J. A* **5**, 307 (1999).
32. W. Cassing and E. Bratkovskaya, *Phys. Rep.* **308**, 65 (1999).
33. V. Koptev *et al.*, *Eur. Phys. J. A* **17**, 235 (2003).
34. V. Franco and R.J. Glauber, *Phys. Rev.* **142**, 1195 (1966).
35. E. Chiavassa *et al.*, *Phys. Lett. B*, **337**, 192 (1994).
36. A. Baldini *et al.*, *Total Cross Sections of High Energy Particles, Vol.12 of Landolt-Börnstein, Numerical Data and Functional Relationships in Science and Technology*, edited by H. Schopper (Springer-Verlag, Berlin, 1988).
37. <http://www-hades.gsi.de/computing/pluto/html/PlutoIndex.htm>.
38. M. Büscher, Proc. XXVIII Mazurian Lakes Conference on Physics, Atomic Nucleus as a Laboratory for Fundamental Processes, 31 August – 7 September 2003, Krzyze, Poland; *Acta Physica Polonica*, in print; arXiv:nucl-ex/0311018.

Appendix

Table 4. Double differential cross sections for $p^{12}\text{C} \rightarrow K^+ X$ reactions obtained with the 1.3 T mode. The errors do not include the systematic uncertainties from the normalisation to pion data.

p_{K^+} (MeV/c)	$d^2\sigma/d\Omega dp$ (nb/(sr MeV/c))			
	$T_p = 1.0$ GeV	1.2 GeV	2.0 GeV	2.3 GeV
171 \pm 11	0.073 \pm 0.027	0.60 \pm 0.18	9.9 \pm 1.8	11.9 \pm 2.9
192 \pm 12	0.073 \pm 0.048	0.88 \pm 0.19	18.6 \pm 1.8	27.9 \pm 4.3
216 \pm 11	0.125 \pm 0.028	1.41 \pm 0.23	24.7 \pm 2.1	45.6 \pm 5.1
240 \pm 12	0.132 \pm 0.032	1.46 \pm 0.21	28.3 \pm 2.3	51.4 \pm 5.4
266 \pm 14	0.178 \pm 0.052	2.47 \pm 0.26	45.7 \pm 2.9	75.5 \pm 6.8
295 \pm 15	0.270 \pm 0.036	2.73 \pm 0.28	54.1 \pm 3.0	89.9 \pm 6.7
325 \pm 15	0.337 \pm 0.045	4.82 \pm 0.41	86.0 \pm 5.4	138 \pm 12
355 \pm 15	0.302 \pm 0.036	6.02 \pm 0.54	99.8 \pm 6.8	158 \pm 13
385 \pm 15	0.330 \pm 0.053	6.76 \pm 0.52	115.9 \pm 7.5	188 \pm 15
415 \pm 15	0.257 \pm 0.038	6.89 \pm 0.61	145 \pm 11	245 \pm 22
445 \pm 15	0.201 \pm 0.066	9.61 \pm 0.85	186 \pm 14	310 \pm 28
475 \pm 15	0.165 \pm 0.047	8.21 \pm 0.61	194.4 \pm 9.5	313 \pm 23
507 \pm 17	0.088 \pm 0.042	6.44 \pm 0.73	220 \pm 12	389 \pm 30

Table 5. Double differential cross sections for $p^{12}\text{C} \rightarrow K^+ X$ reactions obtained with the 1.6 T mode. The errors do not include the systematic uncertainties from the normalisation to pion data.

p_{K^+} (MeV/c)	$d^2\sigma/d\Omega dp$ (nb/(sr MeV/c))		
	$T_p = 1.2$ GeV	1.5 GeV	2.3 GeV
209 \pm 6	1.28 \pm 0.40	14.0 \pm 2.9	73.2 \pm 9.7
233 \pm 6	2.07 \pm 0.50	14.8 \pm 2.7	78 \pm 11
259 \pm 6	2.82 \pm 0.58	17.1 \pm 3.3	105 \pm 17
285 \pm 6	3.51 \pm 0.58	21.5 \pm 3.2	128 \pm 16
315 \pm 6	5.52 \pm 0.77	42.0 \pm 5.0	164 \pm 17
346 \pm 6	6.41 \pm 0.81	48.5 \pm 5.6	238 \pm 24
378 \pm 6	6.96 \pm 0.70	58.0 \pm 5.5	264 \pm 22
415 \pm 6	8.29 \pm 0.70	68.2 \pm 5.6	321 \pm 23
450 \pm 6	7.94 \pm 0.79	77.1 \pm 7.4	351 \pm 31
486 \pm 6	7.24 \pm 0.59	84.4 \pm 6.7	373 \pm 27
521 \pm 6	6.88 \pm 0.53	87.8 \pm 6.5	416 \pm 26
557 \pm 6	6.09 \pm 0.73	99 \pm 11	491 \pm 48
595 \pm 6	4.40 \pm 0.55	82.2 \pm 8.4	428 \pm 38

Table 6. Cross section ratios A/C measured at $T_p = 1.0$ GeV with the 1.3 T mode. The error bars include the statistical and systematic uncertainties.

p_{K^+} (MeV/c)	Ratio	
	Cu/C	Au/C
216 \pm 11	2.05 \pm 1.30	4.65 \pm 3.60
240 \pm 12	3.60 \pm 1.25	5.70 \pm 3.30
266 \pm 14	3.40 \pm 1.10	5.35 \pm 2.55
295 \pm 15	3.95 \pm 0.85	6.20 \pm 1.90
325 \pm 15	3.85 \pm 1.00	6.20 \pm 2.05
355 \pm 15	4.10 \pm 0.95	7.40 \pm 2.05
385 \pm 15	4.65 \pm 0.95	8.25 \pm 2.10
415 \pm 15	4.95 \pm 0.95	9.10 \pm 2.30
445 \pm 15	5.15 \pm 1.50	7.40 \pm 3.20
475 \pm 15	4.10 \pm 1.30	5.50 \pm 2.55
507 \pm 17	4.70 \pm 2.10	10.55 \pm 7.15

Table 7. Cross section ratios Au/C measured at $T_p = 1.5$ with the 1.6 T mode. The error bars include the statistical and systematic uncertainties.

p_{K^+} (MeV/c)	Ratio Au/C
184 ± 8	3.18 ± 0.94
209 ± 11	4.75 ± 0.71
233 ± 11	6.71 ± 0.61
260 ± 12	6.40 ± 0.39
285 ± 13	5.68 ± 0.36
315 ± 14	4.76 ± 0.27
347 ± 14	4.96 ± 0.22
378 ± 14	4.42 ± 0.18
412 ± 14	4.33 ± 0.17
448 ± 14	4.11 ± 0.16
485 ± 15	3.82 ± 0.15
522 ± 15	3.70 ± 0.18
560 ± 16	3.74 ± 0.23
596 ± 16	3.88 ± 0.27

Table 8. Cross section ratios Au/C measured at $T_p = 1.75$ with the 1.6 T mode. The error bars include the statistical and systematic uncertainties.

p_{K^+} (MeV/c)	Ratio Au/C
158 ± 8	1.96 ± 2.00
184 ± 8	4.00 ± 1.41
209 ± 11	6.24 ± 0.73
233 ± 11	9.61 ± 1.02
260 ± 12	8.15 ± 0.49
285 ± 12	7.01 ± 0.42
315 ± 13	6.23 ± 0.33
347 ± 14	5.38 ± 0.24
378 ± 14	4.83 ± 0.20
412 ± 14	4.65 ± 0.18
448 ± 15	4.64 ± 0.18
485 ± 15	4.19 ± 0.16
522 ± 15	4.12 ± 0.18
560 ± 16	3.85 ± 0.21
596 ± 16	3.76 ± 0.24

Table 9. Cross section ratios A/C measured at $T_p = 2.3$ GeV and different D2 operation modes. The error bars include the statistical and systematic uncertainties.

p_{K^+} (MeV/c)	Ratio			
$B = 1.3$ T	1.6 T	Cu/C	Ag/C	Au/C
153 \pm 9		2.54 \pm 0.30	2.62 \pm 0.33	
	158 \pm 8		3.62 \pm 1.11	2.98 \pm 0.82
175 \pm 11		3.63 \pm 0.28	4.21 \pm 0.29	5.40 \pm 2.25
	182 \pm 8		5.53 \pm 0.53	4.96 \pm 0.45
196 \pm 11		3.86 \pm 0.17	5.03 \pm 0.22	7.44 \pm 0.89
	208 \pm 11		6.17 \pm 0.31	8.24 \pm 0.38
218 \pm 11		4.16 \pm 0.14	6.04 \pm 0.20	9.14 \pm 0.72
	233 \pm 11		5.76 \pm 0.25	9.95 \pm 0.40
239 \pm 11		3.86 \pm 0.13	6.07 \pm 0.20	10.84 \pm 0.72
	259 \pm 12		5.77 \pm 0.19	10.05 \pm 0.34
264 \pm 12		3.71 \pm 0.12	5.67 \pm 0.18	9.31 \pm 0.60
	285 \pm 12		5.25 \pm 0.18	8.57 \pm 0.29
293 \pm 14		3.57 \pm 0.10	5.14 \pm 0.14	7.91 \pm 0.47
	315 \pm 13		4.59 \pm 0.15	7.62 \pm 0.25
317 \pm 14		3.228 \pm 0.084	4.51 \pm 0.12	7.18 \pm 0.43
345 \pm 15		3.155 \pm 0.083	4.28 \pm 0.12	6.29 \pm 0.34
	350 \pm 14		4.54 \pm 0.13	6.75 \pm 0.20
376 \pm 15		3.032 \pm 0.076	4.14 \pm 0.11	6.16 \pm 0.34
	380 \pm 14		4.20 \pm 0.11	6.31 \pm 0.18
407 \pm 15		3.010 \pm 0.080	3.94 \pm 0.11	5.27 \pm 0.30
	413 \pm 14		4.00 \pm 0.10	5.74 \pm 0.16
438 \pm 15		2.702 \pm 0.079	3.70 \pm 0.11	4.59 \pm 0.34
	450 \pm 14		3.73 \pm 0.10	5.43 \pm 0.15
468 \pm 15		2.73 \pm 0.10	3.60 \pm 0.13	5.06 \pm 0.34
	487 \pm 15		3.54 \pm 0.09	4.97 \pm 0.14
499 \pm 17		2.49 \pm 0.11	3.48 \pm 0.15	4.63 \pm 0.34
	525 \pm 15		3.45 \pm 0.10	4.68 \pm 0.14
	560 \pm 16		3.17 \pm 0.10	4.50 \pm 0.14
	595 \pm 16		3.26 \pm 0.11	4.45 \pm 0.15

Table 10. Double differential cross section for $pD \rightarrow K^+X$ reactions measured at 1.83 and 2.02 GeV with the 1.45 T and 1.6 T modes, respectively. The errors do not include the overall 20% systematic uncertainty from the determination of the luminosity.

p_{K^+} (MeV/c)	$d^2\sigma/d\Omega dp$ (nb/(sr MeV/c))		
	$B = 1.45$ T	1.6 T	$T_p = 1.83$ GeV
212±12		2.01±0.56	
	212±12		5.4±1.2
236±16		2.34±0.56	
	237±12		7.2±1.4
261±16		5.0±1.1	
	262±12		11.6±2.5
287±12		5.21±0.96	
	289±13		16.2±2.7
319±15		6.49±0.87	
	319±15		16.4±2.9
349±17		10.5±1.2	
	350±16		28.8±2.8
382±14		14.5±1.7	
	381±15		32.9±3.9
415±15		15.8±1.7	
	413±15		42.9±4.2
449±17		19.1±1.7	
	449±17		47.5±4.1
485±17		22.2±1.9	
	484±17		52.9±5.0
521±18		33.0±3.9	
	519±17		60.8±7.0
554±12		29.0±3.4	
	555±18		70.0±7.5
587±15		29.1±3.4	
	591±18		68.6±7.8

Table 11. Relevant reaction channels for K^+ production on deuterons and the corresponding total cross sections calculated according to the parameterisation taken from Ref. [7].

Reaction	σ (μ b)	
	$T_p = 1.83$ GeV	2.02 GeV
$pp \rightarrow \Lambda K^+ p$	3.85	10.9
$pn \rightarrow \Lambda K^+ n$	7.12	19.4
$pp \rightarrow \Sigma^0 K^+ p$	0.005	1.36
$pn \rightarrow \Sigma^0 K^+ n$	0.008	1.68
$pp \rightarrow \Sigma^+ K^+ n$	0.001	0.52
$np \rightarrow \Sigma^- K^+ p$	0.010	2.78